Chapter 3

Two-mode interference coupler based on SPP waveguide

Contents

3.1 Introduction 60

3.2 Surface plasmon polariton based two-mode interference waveguide coupler 60

3.3 SPP mode analysis in optical waveguide 62

3.3.1 Effective index method 63

3.3.2 Estimation of modes by effective index method 65

3.3.3 Modes in SPP based waveguide 66

3.3.4 Mode propagation of two-mode waveguide 69

3.4 Optical pulse controlled surface plasmonic two-mode interference (SPTMI) waveguide coupler . . . 73

3.4.1 Wavelength dependence of SPTMI waveguide coupler 75

3.4.2 Optical pulse controlled behavior of SPTMI waveguide coupler 77

3.4.3 Power transferred to output waveguides 84

3.4.4 Total length of SPTMI coupler 88

3.4.5 Fabrication tolerance 90

3.4.6 Optical power launching efficiency 91

3.5 Values of device parameters of the proposed device . 93

3.6 Conclusion 95

3.1 Introduction

As mentioned in chapter 2, compact optical components have become indispensable to achieve large scale integration of integrated optical processors used to provide optical processing of present day's high speed communication system. In this direction, two-mode interference (TMI) coupler has become strong candidate for integrated optical device components due to its compactness and simple structure [115]. In recent years, surface plasmon polariton (SPP) waveguide has been attracted for integrated optical devices due to their compactness and easy fabrication [12, 13, 116]. Surface plasmon polaritons (SPPs) offer confinement of electromagnetic energy in the metal-dielectric interface [117] and the possibility to realize ultra-compact optical signal processing components. For faster operation of the integrated optic devices, all-optical control of the device components has become another essential requirement. There are many approaches such as Mach-Zehnder based nonlinear two-mode interference waveguide [118], distributed bragg reflector based quantum dots [119], nonlinear directional coupler based multimode interference (NDCMMI) coupler [120], MZ-MMI coupler [121], optically-controlled two-mode interference (OTMI) coupler with nonlinear cladding [122] etc. to achieve optical control of integrated optical devices.

In this chapter, an ultra-compact surface plasmonic two mode interference (SPTMI) waveguide has been introduced as a basic component for integrated optical processor devices. Mathematical analysis of the SPTMI waveguide has been carried out using a mathematical model based on effective index methods. Dependence of mode propagation on the device parameters are shown in the chapter. The optical pulse dependent coupling behavior of the SPTMI coupler is discussed and compared with previously reported works. The fabrication tolerance of the device is also discussed.

3.2 Surface plasmon polariton based two-mode interference waveguide coupler

Fig-3.1 shows the schematic view of the surface plasmonic two-mode interference (SPTMI) waveguide coupler. It consists of a two mode interference region of width $2w$ and thickness t, and two single mode input access waveguides and two single mode output access waveguides having core of width w and same thickness t. The device is made up of the following materials:

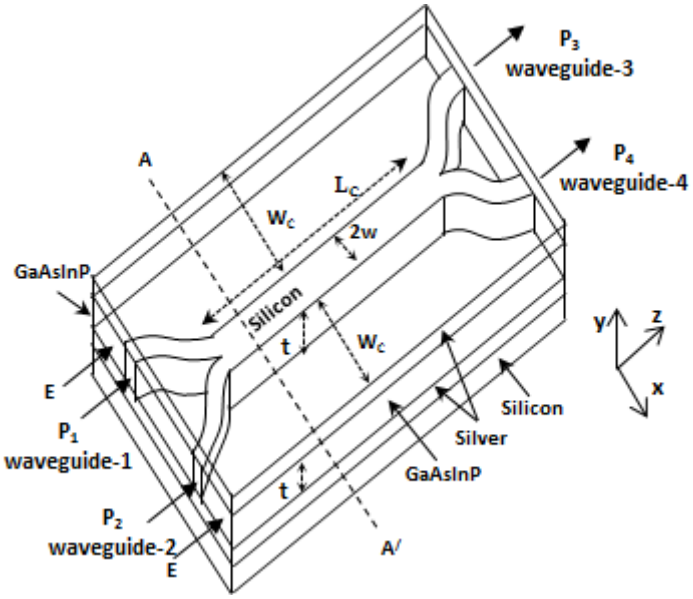

(a) Three dimensional view

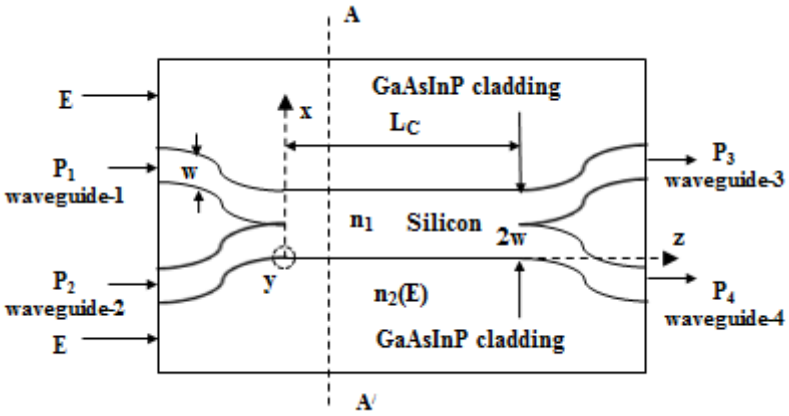

(b) Top view

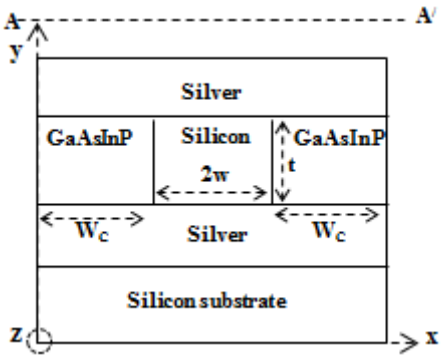

(c) Cross sectional view along the line $AA^{/}$

Figure 3.1: Schematic view of optically-controlled, surface plasmonic two mode interference (SPTMI) coupler with core width $2w$, thickness t and coupling length L_C.

- **Core:** The core of the SPTMI device is made up of silicon having refractive index $n_1 = 3.5$ [123].

- **Side claddings:** The material in the left and right cladding is GaAsInP which shows a nonlinear refractive index change with a fast response time $\sim 1ps$. The refractive index can be expressed as a function of the applied optical pulse of energy E and is written as follows [122, 124]

$$n_2(E) = n_2(0) + \frac{n_{nl}E}{1.605A_{clad}T_P} \tag{3.1}$$

  where, $n_2(0) = 3.17$ is the refractive index of GaAsInP when no optical pulse is applied. $n_{nl} = -2 \times 10^{-3}\mu m^2 W^{-1}$ is the nonlinear refractive index coefficient of GaAsInP and T_P is the full width at half maximum of pulse. $A_{clad} = 2W_C t$ is the area of cladding on which optical pulse is applied where W_C is the cladding width at left and right side.

- **Top and bottom claddings:** The top and bottom claddings are made up of silver which is a lossy material. The refractive index of silver for some frequently used wavelengths are given below [123]

$$\begin{aligned} n_m &= n_{m,real} + n_{m,im} \\ &= 0.514 + 10.80j \qquad \lambda = 1.550\mu m \\ &= 0.394 + 8.2j \qquad \lambda = 1.330\mu m \\ &= 0.226 + 6.990j \qquad \lambda = 1.033\mu m \\ &= 0.143 + 5.090j \qquad \lambda = 0.7749\mu m \\ &= 0.119 + 3.964j \qquad \lambda = 0.6328\mu m \end{aligned}$$

  Here, $n_{m,real}$ and $n_{m,im}$ denote the real and imaginary parts of the complex refractive index n_m. Since operating wavelength is used as $\lambda = 1.330\mu m$, the refractive index of silver is chosen to be $n_m = 0.394 + 8.2j$.

3.3 SPP mode analysis in optical waveguide

Surface plasmon polariton (SPP) are electromagnetic surface waves which propagate at the interface separating a dielectric medium and a conducting medium [12]. These surface waves arise due to coupling of electromagnetic field to oscillations of free electrons in the metal surface and decay exponentially as one moves

in a direction perpendicular to the interface [12]. When light is incident at a metal-insulator-metal (MIM) waveguides, bound SPP modes are excited in each single interface. If the separation between adjacent metal-insulator interfaces is smaller than or comparable to the decay length of the bound SPP modes, the bound SPP modes interact and the interaction gives rise to coupled modes. The propagation constants for the coupled SPP modes can be written as

$$\beta_m(n_1, n_m, n_2(E)) = \beta_m^r(n_1, n_m, n_2(E)) + j\beta_m^{im}(n_1, n_m, n_2(E)) \tag{3.2}$$

where, $m = 0, 1, 2, 3.....$ denote the mode number. Above equation can be written in simplified form as follows

$$\beta_m(n_2(E)) = \beta_m^r(n_2(E)) + j\beta_m^{im}(n_2(E)), \quad m = 0, 1, 2, 3..... \tag{3.3}$$

3.3.1 Effective index method

Effective index method is one of the most widely used approaches to describe mode propagation in integrated optic waveguide devices [45, 49]. By using effective index method, a three dimensional waveguide can be analyzed by considering it as combination of two-dimensional waveguides. The same approach can be used for the modeling of surface plasmon polariton modes guided by the various waveguide structures. Fig-3.2 shows the cross sectional view of the SPTMI waveguide coupler. With the help of the effective index method, the waveg-

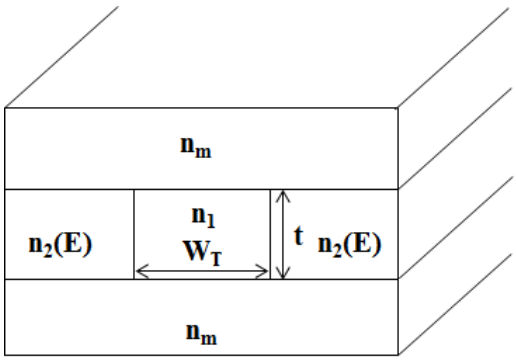

Figure 3.2: Schematic view of the SPTMI waveguide with core width W_T and core thickness t

uide shown in Fig-3.2 can be approximated as a combination of two dimensional waveguides by the following two methods.

The x-method of effective index modelling:

The x-method of effective index modeling of a three dimensional SPTMI waveguide has been illustrated in Fig-3.3. In this method, the waveguide shown in

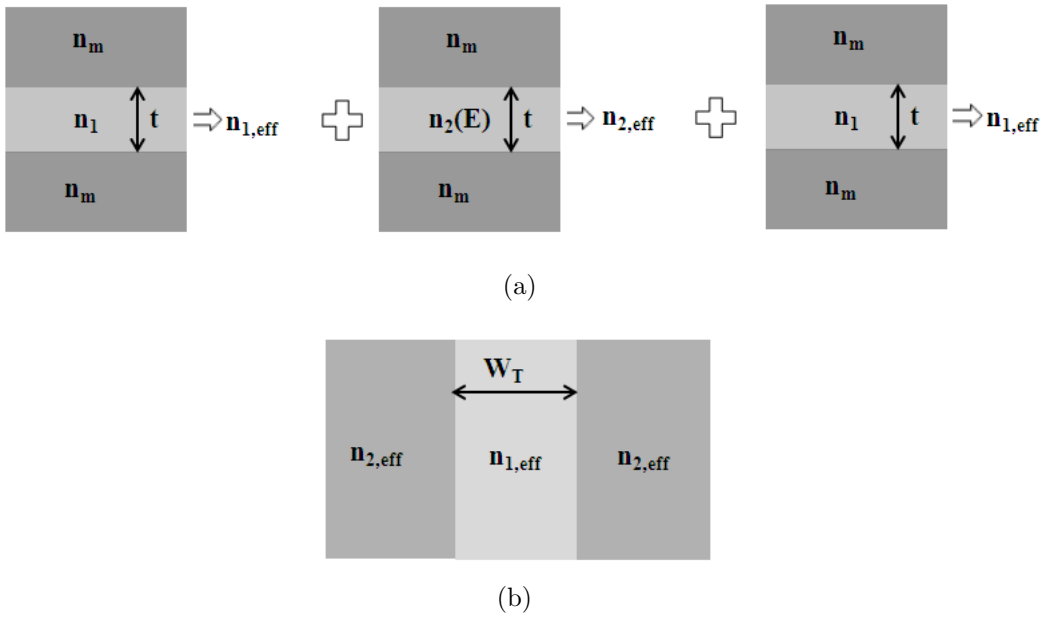

Figure 3.3: x-method for effective index modeling of SPTMI waveguide.

Fig-3.2 can be approximated as a combination of a set of two dimensional waveguides of thickness t, cladding index n_m and core effective indices n_1 and $n_2(E)$ as shown in Fig-3.3(a) and a two dimensional waveguide of width W_T, core effective index $n_{1,eff}$ and cladding effective index $n_{2,eff}$ as shown in Fig-3.3(b). Here, $n_{1,eff}$ and $n_{2,eff}$ are the effective refractive indices of the core dielectric and the nonlinear material respectively, sandwiched between the metal cladding in the y-direction.

The y-method of effective index modelling:

The y-method of effective index modeling of a three dimensional SPTMI waveguide has been illustrated in Fig-3.4. In this method, the waveguide shown in Fig-3.2 can be approximated as a combination of the two dimensional waveguide of width W_T, core effective index n_1 and cladding effective index $n_2(E)$ (as shown in Fig-3.4(a)) and the two dimensional waveguide of thickness t, core effective index $n^{/}_{eff}$ and cladding index n_m (as shown in Fig-3.4(b)) where, $n^{/}_{eff}$ is the effective refractive index of the core dielectric of refractive index n_1 sandwiched between the nonlinear cladding material of refractive index $n_2(E)$ on the

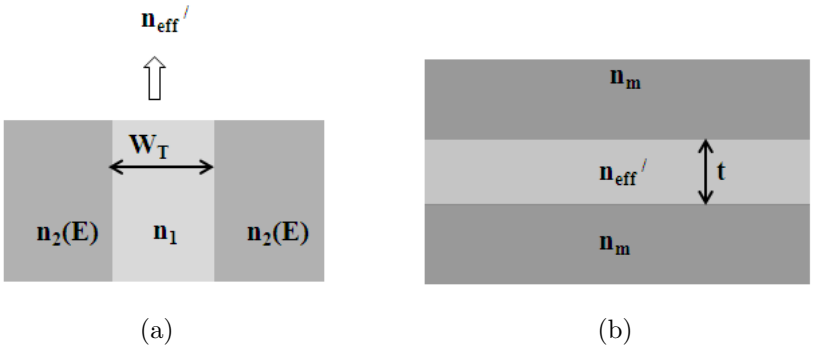

Figure 3.4: y-method for effective index modeling of SPTMI waveguide.

x-direction.

3.3.2 Estimation of modes by effective index method

In our work, the three dimensional SPTMI coupler has been analyzed with the help of y-method of effective index modeling. The effective refractive indices $n_{m,r}^{eff}(E)$ for mode propagation in the SPTMI coupler shown in Fig-3.2, consisting of core dielectric with refractive index n_1, core width W_T and core thickness t, the nonlinear cladding on x-direction with refractive index $n_2(E)$ and the metal cladding on y-direction with refractive index n_m can be estimated with the help of effective index method and dispersion equation for MIM structure described in section 2.2.1 of previous chapter, as follows:

The dispersion equation along x-direction can be written as

$$V_I\sqrt{1-b_I} = (m+1)\pi - 2\tan^{-1}\sqrt{\frac{1-b_I}{b_I}} \tag{3.4}$$

where m is an integer. V_I and b_I are the normalized frequency and normalized guide index of the waveguide given by

$$\begin{aligned} V_I &= k_0 W_T\sqrt{n_1^2 - n_2(E)^2} \\ b_I &= \frac{n_{eff}^{/2} - n_2(E)^2}{n_1^2 - n_2(E)^2} \end{aligned} \tag{3.5}$$

$n_{eff}^{/}$ is the effective refractive index along x-direction. Substituting value of b_I which satisfy equation (3.4) into equation (3.5), $n_{eff}^{/}$ can be estimated as

$$n_{eff}^{/} = \sqrt{n_2(E)^2 + b_I(n_1^2 - n_2(E)^2)} \tag{3.6}$$

The dispersion equation for the MIM waveguide in y-direction, shown in Fig-3.2 can be written for odd parity, as follows [125]

$$\beta_m \approx k_0 \sqrt{\epsilon_{eff}^{/} + \frac{2\epsilon_{eff}^{/}\sqrt{\epsilon_{eff}^{/} - \epsilon_m}}{k_0 t(-\epsilon_m)}} \tag{3.7}$$

where $\epsilon_m = n_m^2$ is the relative permittivity of the metal and $\epsilon_{eff}^{/} = n_{eff}^{/2}$ is the effective relative permittivity of the core. Substituting the values of ϵ_m and $\epsilon_{eff}^{/}$, the complex propagation constant β_m can be estimated from equation (3.7). Knowing β_m, the effective refractive index $n_{m,r}^{eff}$ and propagation length can be estimated from the following relations:

$$n_{m,r}^{eff} = \frac{\text{real}(\beta_m)}{k_0} \tag{3.8}$$

$$L_{P,m} = \frac{1}{2\text{imag}(\beta_m)} \tag{3.9}$$

3.3.3 Modes in SPP based waveguide

We have studied the modal characteristics of the SPTMI coupler with respect to variations in different waveguide parameters with the help of effective index methods. Fig-3.5 shows variation of the real part of propagation constant (β_m^r, $m = 0, 1, 2...$) of the various SPP modes propagating through the coupling region versus core width (W_T) obtained by effective index method with core thickness $t = 5.0\mu m$, $n_1 = 3.5$ (silicon), $n_2(0) = 3.17$ (GaAsInP) and $n_m = 0.394 + 8.2j$ (silver) at the wavelength $\lambda = 1.33\mu m$. It is seen from the figure that as W_T increases, higher order modes start appearing along with the fundamental mode. It is apparent from the figure that the first order mode starts appearing at $W_T = 0.45\mu m$, the second order mode appears at $W_T = 0.90\mu m$, and so on. Thus, the device works in two-mode region for values of W_T in the range $0.45\mu m - 0.90\mu m$. For $W_T \geq 0.90\mu m$, the second order mode starts appearing and the device no longer works in two-mode region. Fig-3.6 shows variation of real part of effective refractive indices ($n_{m,r}^{eff} = \beta_m^r/k_0$, $m = 0, 1, 2...$) of the various SPP modes versus core width obtained by effective index method with $t = 5.0\mu m$, $\lambda = 1.33\mu m$, $n_1 = 3.5$, $n_2(0) = 3.17$ and $n_m = 0.394 + 8.2j$. It is apparent from the figure that for two-mode interference coupling in the device, the core width should range between $0.45\mu m$ to $0.90\mu m$, as also seen from Fig-3.5.

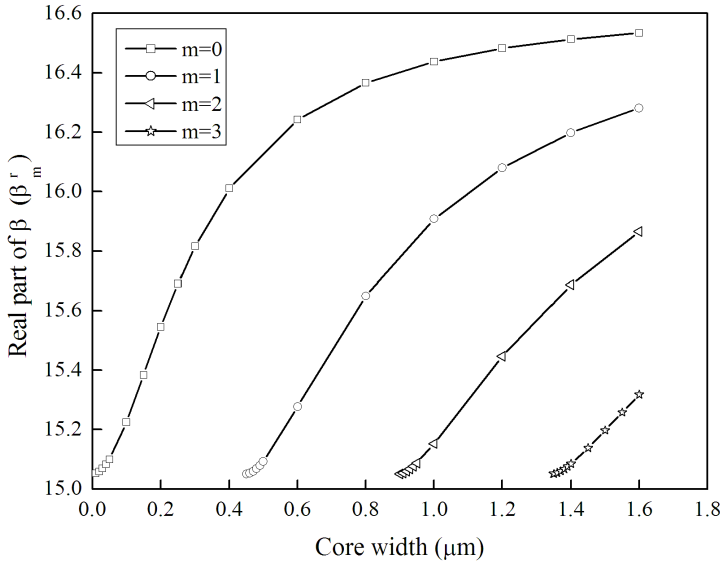

Figure 3.5: Real part of propagation constant (β_m^r) versus core width with $t = 5.0\mu m$, $\lambda = 1.33\mu m$, $n_2(0) = 3.17$, $n_m = 0.394 + 8.2j$ and $n_1 = 3.5$.

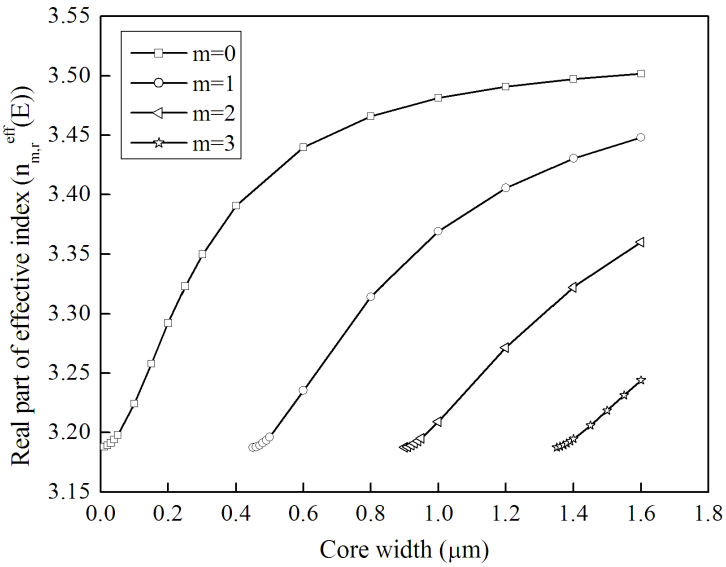

Figure 3.6: Real part of effective refractive index ($n_{m,r}^{eff}$) versus core width with $t = 5.0\mu m$, $\lambda = 1.33\mu m$, $n_2(0) = 3.17$, $n_m = 0.394 + 8.2j$ and $n_1 = 3.5$.

The variation of the imaginary part of propagation constant (β_m^{im}, $m = 0, 1, 2...$) of the propagating modes versus core width (W_T) obtained by effective index method is shown in Fig-3.7 for $t = 5.0\mu m$, $n_1 = 3.5$, $n_2(0) = 3.17$ and $n_m = 0.394 + 8.2j$ at the wavelength $\lambda = 1.33\mu m$. It is found that, as the core width increases, the imaginary part of the propagation constant also increases. For larger core width, the effective surface area of the metallic contact in the SPTMI coupler is also larger. The corresponding increase in material loss due to presence of silver may be accounted for the increase in the imaginary part of

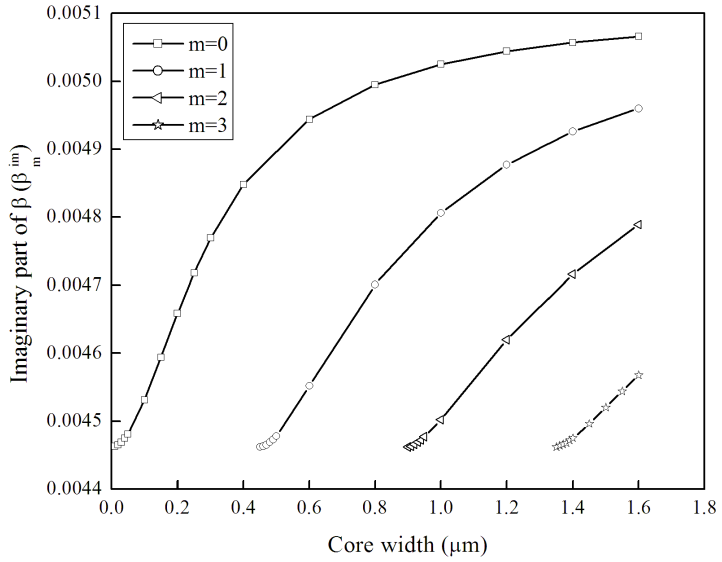

Figure 3.7: Imaginary part of propagation constant (β_m^{im}) versus core width with $t = 5.0\mu m$, $\lambda = 1.33\mu m$, $n_2(0) = 3.17$, $n_m = 0.394 + 8.2j$ and $n_1 = 3.5$.

propagation constant with increase in core width W_T. Fig-3.8 shows variation

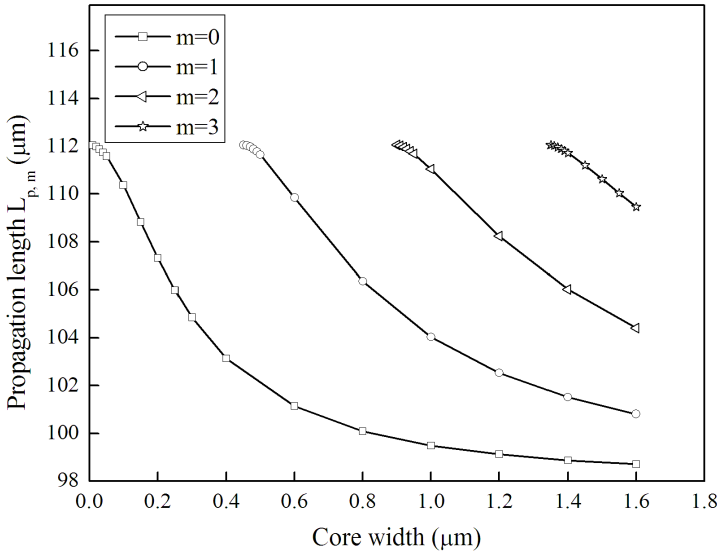

Figure 3.8: Propagation length ($L_{P,m}$) versus core width with $t = 5.0\mu m$, $\lambda = 1.33\mu m$, $n_2(0) = 3.17$, $n_m = 0.394 + 8.2j$ and $n_1 = 3.5$.

of the propagation length ($L_{P,m} = 1/(2\beta_m^{im})$, $m = 0, 1, 2...$) of the various SPP modes versus core width (W_T) obtained by effective index method with $t = 5.0\mu m$, $n_1 = 3.5$, $n_2(0) = 3.17$ and $n_m = 0.394 + 8.2j$ at the wavelength $\lambda = 1.33\mu m$. From the figure, it is apparent that the propagation length of the various modes decreases as the core width increases i.e., the larger is the core width, the more will be the energy dissipation of the propagating modes and the SPP wave

will die out earlier at a smaller coupling distance.

3.3.4 Mode propagation of two-mode waveguide

Fig-3.9 shows the variation of real part of propagation constant (β_m^r, $m = 0, 1, 2...$) of the SPP modes propagating in the coupling region versus core thickness with $W_T = 0.48\mu m$ for two-mode coupling, $\lambda = 1.33\mu m$, $n_2(0) = 3.17$, $n_m = 0.394 + 8.2j$ and $n_1 = 3.5$. It is evident from the figure that for

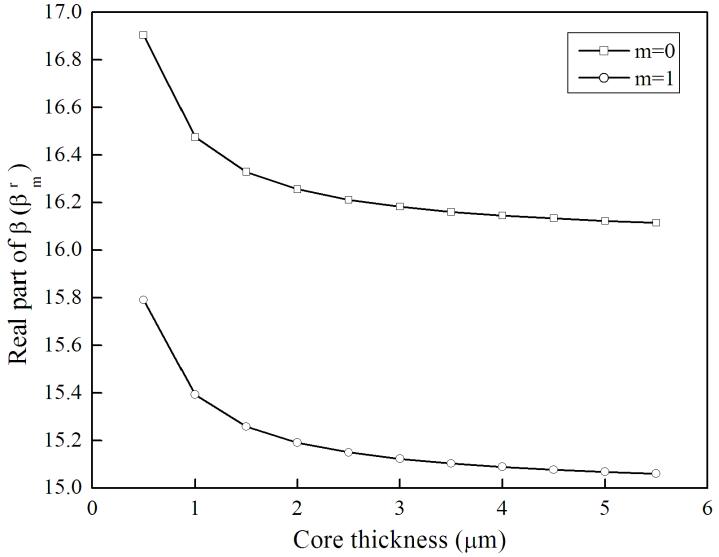

Figure 3.9: Real part of propagation constant (β_m^r) versus core thickness with $W_T = 0.48\mu m$, $\lambda = 1.33\mu m$, $n_2(0) = 3.17$, $n_m = 0.394 + 8.2j$ and $n_1 = 3.5$.

$W_T = 0.48\mu m$, only the fundamental and the first order modes propagate through the coupling region and the number of propagated modes is independent of core thickness t. It is also seen from the figure that, as the core thickness increases, the real part of the propagation constant decreases. Similar behavior is seen in the variation of the real part of effective index of the propagating modes with respect to variations in the core thickness. Fig-3.10 shows the variation of the real part of effective refractive indices ($n_{m,r}^{eff}$, $m = 0, 1, 2...$) of the fundamental and first order modes versus core thickness with $W_T = 0.48\mu m$, $\lambda = 1.33\mu m$, $n_2(0) = 3.17$, $n_m = 0.394 + 8.2j$ and $n_1 = 3.5$. It is evident from the figure that, as the core thickness increases, the real part of effective index of the individual modes decreases rapidly for small values of t and then with a steady rate for larger values of t.

The variation of the imaginary part of propagation constant of the fundamental and first order SPP modes with respect to variations in the core thickness

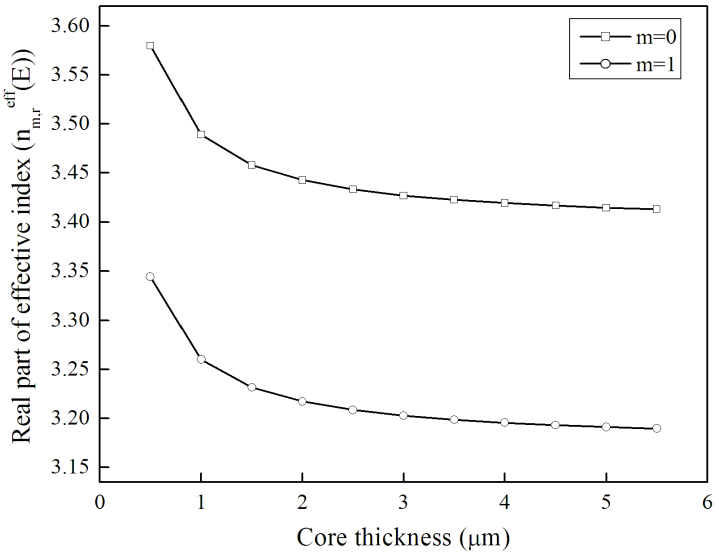

Figure 3.10: Real part of effective refractive index ($n_{m,r}^{eff}$) versus core thickness with $W_T = 0.48\mu m$, $\lambda = 1.33\mu m$, $n_2(0) = 3.17$, $n_m = 0.394 + 8.2j$ and $n_1 = 3.5$.

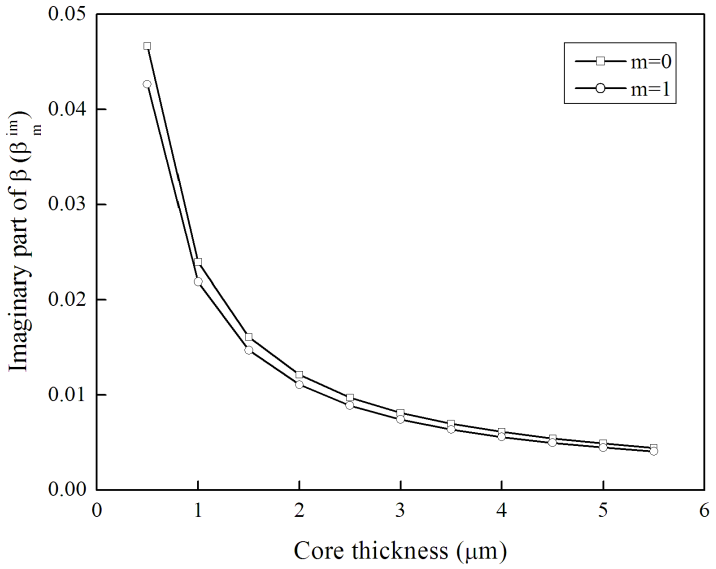

Figure 3.11: Imaginary part of propagation constant (β_m^{im}) versus core thickness with $W_T = 0.48\mu m$, $\lambda = 1.33\mu m$, $n_2(0) = 3.17$, $n_m = 0.394 + 8.2j$ and $n_1 = 3.5$

is shown in Fig-3.11. It is found that the imaginary part of propagation constant decreases rapidly with increase in core thickness in the range $0\mu m$ to $1\mu m$. For $t \geq 1\mu m$, the rate of decrease of imaginary part of propagation constant with increase in core thickness gradually decreases and becomes steady for t values in the range $4\mu m$ to $6\mu m$. Fig-3.12 shows the variation in the propagation length for SPP fundamental and first order modes with respect to the core thickness. It is seen that the propagation length of the two propagating modes increases almost linearly as the core thickness increases i.e., the larger is the core thickness,

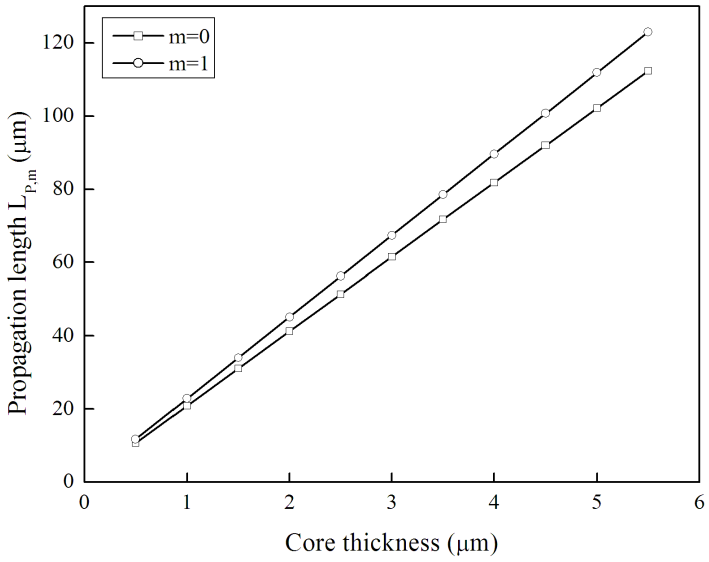

Figure 3.12: Propagation length ($L_{P,m}$) versus core thickness with $W_T = 0.48\mu m$, $\lambda = 1.33\mu m$, $n_2(0) = 3.17$, $n_m = 0.394 + 8.2j$ and $n_1 = 3.5$

the smaller is the energy dissipation of the propagating modes and the SPP wave travels larger distance before the intensity dies out.

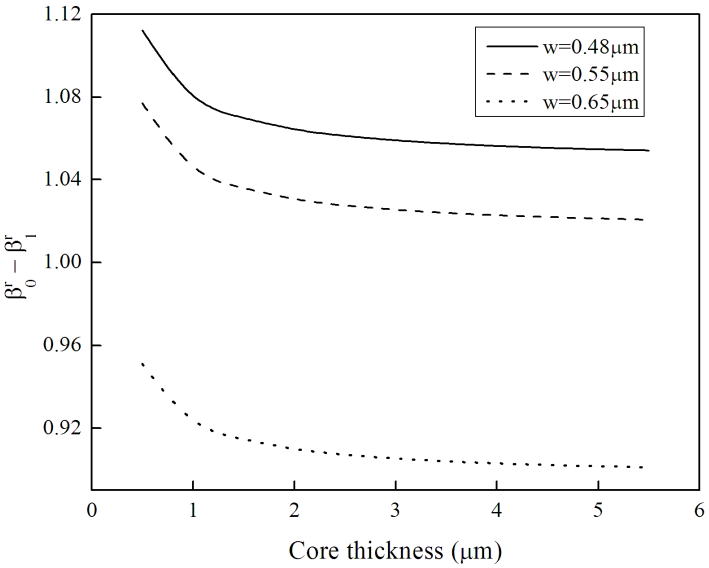

Figure 3.13: Difference of real part of propagation constants of fundamental and first order modes versus the core thickness with $n_1 = 3.5$, $n_2(0) = 3.17$, $n_m = 0.394 + 8.2j$ and $\lambda = 1.33\mu m$ and for core width $W_T = 0.48\mu m$, $0.55\mu m$ and $0.65\mu m$.

Fig-3.13 represents the variation in the difference of real parts of propagation constants of fundamental and first order modes versus the core thickness with $n_1 = 3.5$, $n_2(0) = 3.17$, $n_m = 0.394 + 8.2j$ and $\lambda = 1.33\mu m$ for core width $W_T = 0.48\mu m$, $0.55\mu m$ and $0.65\mu m$ within the two-mode coupling region. It is

seen that the difference of real parts of propagation constants of fundamental and first order modes first decreases rapidly for t variation in the range 0 to $2\mu m$ and then gradually becomes steady for any further increase of t. It is also seen that, as the core width W_T increases, the difference of real parts of propagation constants of the two modes decreases. The beat length of the device depends inversely on the magnitude of this difference $(= \pi/(\beta_0^r - \beta_1^r))$. The smaller is the core width (W_T), the larger is the difference of real parts of propagation constants of fundamental and first order modes, and the smaller is the beat length of the device.

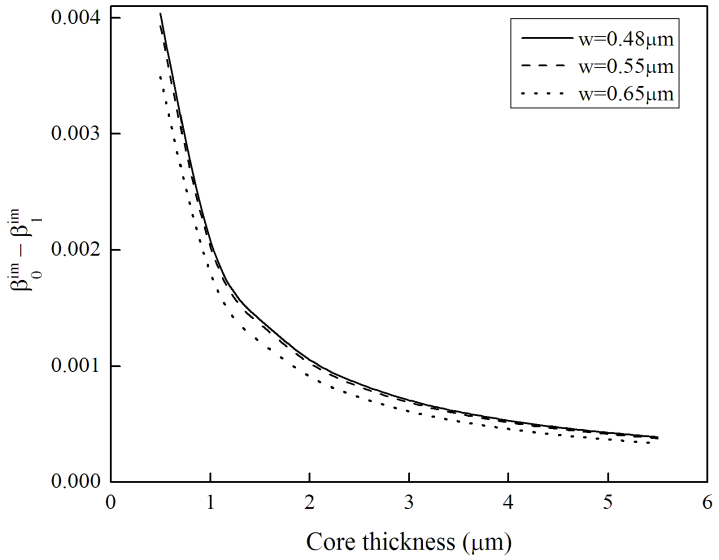

Figure 3.14: Difference of imaginary parts of propagation constants of fundamental and first order modes versus core thickness with $n_1 = 3.5$, $n_2(0) = 3.17$, $n_m = 0.394 + 8.2j$ and $\lambda = 1.33\mu m$ and for core width $W_T = 0.48\mu m$, $0.55\mu m$ and $0.65\mu m$.

Fig-3.14 shows the difference of imaginary parts of propagation constants of fundamental and first order SPP modes versus core thickness t with $n_1 = 3.5$, $n_2(0) = 3.17$, $n_m = 0.394 + 8.2j$ and $\lambda = 1.33\mu m$ for core width $W_T = 0.48\mu m$, $0.55\mu m$ and $0.65\mu m$. It is found that difference of imaginary parts of propagation constants of the two SPP modes decreases as t increases. The rate of change of $(\beta_0^{im} - \beta_1^{im})$ is rapid at first and becomes constant for core thickness larger than $4\mu m$ $(t \geq 4\mu m)$. On the other hand, the variation of core width has negligible effect on the variation of the difference of imaginary parts of propagation constants.

3.4 Optical pulse controlled surface plasmonic two-mode interference (SPTMI) waveguide coupler

To understand the basic principle of the SPTMI waveguide device (as shown in Fig-3.1), we consider that the input field is launched through only on input access waveguide. The input field $H_1(x,0)$ is summation of the mode field distribution of the two excited modes and represented approximately as follows [122]

$$H_1(x,0) = \sum_{m=0}^{1} b_m^T H_m(x) \tag{3.10}$$

where $H_m(x)$ is the mode field of the mth excited mode of TMI region at $z = 0$. b_m^T is the mth mode field excitation coefficient of the proposed plasmonic TMI coupler and can be estimated from Fourier series coefficients of odd periodic functions.

The mode fields at output waveguide-3 and waveguide-4 at $z = L$ are assumed to be single mode and contributed by excited modes. These output fields at output access waveguide-3 and output access waveguide-4 are respectively written as the following:

$$H_3(x,L,E) = \left[\sum_{m=0}^{1} c_{3,m}^T H_m(x) \exp\left[j\{\beta_0^r(n_2(E)) - \beta_m^r(n_2(E))\}L\right] \exp\left[-\beta_m^{im}(n_2(E))L\right]\right] \exp\left[-j\beta_0^r(n_2(E))L\right] \tag{3.11}$$

$$H_4(x+w,L,E) = \left[\sum_{m=0}^{1} c_{4,m}^T H_m(x+w) \exp\left[j\{\beta_0^r(n_2(E)) - \beta_m^r(n_2(E))\}L\right] \exp\left[-\beta_m^{im}(n_2(E))L\right]\right] \exp\left[-j\beta_0^r(n_2(E))L\right] \tag{3.12}$$

where, $c_{3,m}^T$ and $c_{4,m}^T$ are the coefficients of the field contribution of mth mode for third and fourth waveguide respectively and can be evaluated by using a simple model based on SPP sinusoidal modes.

When light is incident through input access waveguide-1, two surface plasmon polariton (SPP) fundamental and first order modes are excited in metal-insulator-metal (MIM) TMI region. Since the two excited SPP modes propagate

through the TMI region with different propagation constants, a phase difference is observed between the two propagating modes at the end of the coupling region. When optical pulse energy is applied at the GaAsInP cladding region resulting in refractive index modulation of the cladding, an additional phase shift $\Delta\Phi(E)$ is induced between the excited SPP modes propagating through the silicon core. The resultant phase difference between the two modes at the end of the coupling region after application of optical pulse of energy E can be written as

$$\begin{aligned}\Delta\Phi_T(E) &= \left[\beta_0^r(n_2(E)) - \beta_1^r(n_2(E))\right] L \\ &= \left[\beta_0^r(n_2(0)) - \beta_1^r(n_2(0))\right] L \\ &\quad + \left[\Delta\beta_{1,r}^{eff}(n_2(E)) - \Delta\beta_{0,r}^{eff}(n_2(E))\right] L \end{aligned} \tag{3.13}$$

The first term in equation (3.13) is the phase difference between the two excited modes without application of optical pulse energy, whereas the second term is the phase difference due to application of energy E. Here, $\beta_0^r(n_2(0))$ and $\beta_1^r(n_2(0))$ are the real parts of propagation constants for fundamental and first order modes obtained without launching optical pulse into GaAsInP cladding. $\Delta\beta_{0,r}^{eff}(n_2(E))$ and $\Delta\beta_{1,r}^{eff}(n_2(E))$ are respectively the change in the real part of propagation constants of fundamental mode and first order mode due to application of optical pulse energy.

Substituting $\beta = n(2\pi/\lambda)$, equation (3.13) can be written as

$$\Delta\Phi_T(E) = \left[\beta_0^r(n_2(0)) - \beta_1^r(n_2(0))\right] L + \frac{2\pi L}{\lambda}\left[\Delta n_{1,r}^{eff}(E) - \Delta n_{0,r}^{eff}(E)\right] \tag{3.14}$$

where, $\Delta n_{0,r}^{eff}(E)$ and $\Delta n_{1,r}^{eff}(E)$ are effective real refractive index change of fundamental mode and first order mode respectively and can be written as follows

$$\begin{aligned}\Delta n_{0,r}^{eff}(E) &= n_{0,r}^{eff}(0) - n_{0,r}^{eff}(E) \\ \Delta n_{1,r}^{eff}(E) &= n_{1,r}^{eff}(0) - n_{1,r}^{eff}(E)\end{aligned} \tag{3.15}$$

Here, $n_{0,r}^{eff}(0)$ and $n_{1,r}^{eff}(0)$ denote the real effective refractive indices of the fundamental mode and the first order mode respectively when no optical pulse is applied at the cladding region, whereas $n_{0,r}^{eff}(E)$ and $n_{1,r}^{eff}(E)$ represent the real effective refractive indices of the fundamental mode and the first order mode respectively after the application of optical pulse of energy E.

From equation (3.14), phase change due to application of energy E is

obtained as

$$\Delta\Phi(E) = \frac{2\pi L}{\lambda}\left[\Delta n_{1,r}^{eff}(E) - \Delta n_{0,r}^{eff}(E)\right] \tag{3.16}$$

When the phase shift induced due to the applied optical pulse is equal to π i.e., $\Delta\Phi(E) = \pi$, the corresponding length of coupling region is known as coupling length (L_C). For $L = L_C$, equation (3.16) can be written as

$$\frac{2\pi L_C}{\lambda}\left[\Delta n_{1,r}^{eff}(E) - \Delta n_{0,r}^{eff}(E)\right] = \pi$$

$$\text{or,} \qquad L_C = \frac{\lambda}{2\left[\Delta n_{1,r}^{eff}(E) - \Delta n_{0,r}^{eff}(E)\right]} \tag{3.17}$$

Equation (3.17) gives the expression for the length of TMI region required to get π phase shift due to application of optical pulse of energy E. L_C can be estimated by using equations (3.15) and (3.17) along with the following equation:

$$n_{m,r}^{eff}(E) = \beta_m^r(\frac{\lambda}{2\pi}), \quad m = 0, 1 \tag{3.18}$$

where, β_m^r can be estimated from equation (3.7) as discussed in section 3.3.2.

3.4.1 Wavelength dependence of SPTMI waveguide coupler

The wavelength of operation has a considerable effect on the propagation and loss of the various propagating modes as well as the device parameters. We have studied the dependence of refractive indices of the materials used and device parameters on the wavelength of operation. Table-3.1 shows the refractive indices of the materials [123] used in the SPTMI coupler. The Table-3.1 also shows the coupling length of the device and the propagation length of the two propagating modes for a width (W_T) corresponding to two-mode propagation, GaAsInP cladding refractive index $n_2(E) = 3.17$ and change in GaAsInP cladding refractive index $\Delta n_2(E) = 0.01$.

It is seen from the table that, as the operating wavelength increases, a larger core width is required to allow two-mode propagation in the coupling region. Moreover, with increase in the operating wavelength and core width of coupling region for two-mode propagation, the coupling length (length of coupling region required to introduce additional phase change of π by application of

Table 3.1: Wavelength dependence of device parameters

Wavelength λ (μm)	Refractive index of silicon n_1	Refractive index of metal (silver) n_m	Core width W_T (μm)	Coupling length L_C (μm)	Prop. length for 0th order mode $L_{P,0}$ (μm)	Prop. length for 1st order mode $L_{P,1}$ (μm)
0.6328	3.880	$0.119+3.964j$	0.15	42.53	32.12	41.26
0.7293	3.752	$0.148+4.74j$	0.20	54.47	43.93	53.40
0.8266	3.673	$0.145+5.5j$	0.25	65.24	68.16	79.99
1.120	3.536	$0.251+7.67j$	0.40	88.66	94.64	104.92
1.330	3.502	$0.394+8.2j$	0.48	92.35	102.16	111.89
1.400	3.488	$0.421+8.37j$	0.51	96.74	100.83	110.31
1.512	3.481	$0.455+9.08j$	0.55	101.06	113.0	122.7
1.550	3.478	$0.469+9.32j$	0.58	110.06	116.4	126.2
1.590	3.472	$0.485+9.57j$	0.60	112.46	119.8	129.6

optical pulse, so as to change cross state coupling of device to bar state coupling) also increase. In other words, as the wavelength increases, the device dimensions also increase in both lateral and propagation directions.

On the other hand, at lower wavelength ($\lambda \leq 0.5\mu m$), silicon has a large value of absorption coefficient (imaginary part of refractive index) [123] which may lead to dissipation of energy of the propagating modes. This is evident from the smaller values of propagation length in the device at lower wavelengths,

as seen in Table-3.1. As the wavelength increases, the absorption coefficient decreases gradually and at $\sim 1.33\mu m$, the absorption coefficient of silicon is zero [123] and silicon behaves as a perfect dielectric with negligible propagation loss.

Thus, in order to ensure a compact device size as well as a smaller propagation loss, we select the operating wavelength as $\lambda = 1.33\mu m$ which is a crucial wavelength for telecommunication purposes.

3.4.2 Optical pulse controlled behavior of SPTMI waveguide coupler

When an optical pulse of energy E is incident on GaAsInP cladding region, index modulation of GaAsInP occurs. This change in GaAsInP cladding refractive index caused by the applied optical pulse affects the propagation constant of the SPP fundamental mode and first order mode propagating along silicon-silver interfaces and introduces an additional phase difference between the two modes. The dependence of effective refractive index change ($\Delta n_{m,r}^{eff}(E)$) produced by applied optical pulse of energy E for fundamental and first order SPP modes on the core width(W_T) is shown in Fig- 3.15 for $t = 5.0\mu m$, $\lambda = 1.33\mu m$, $n_2(0) = 3.17$, $n_m = 0.394 + 8.2j$ and $n_1 = 3.5$. It is seen that effective refractive index

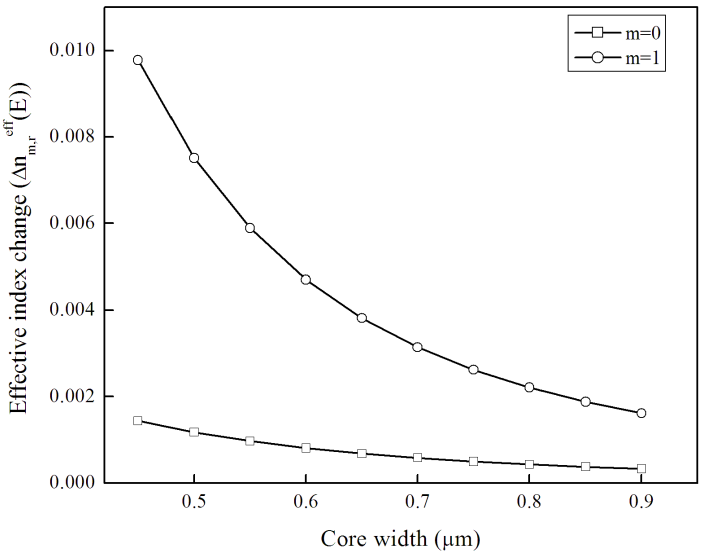

Figure 3.15: Effective refractive index change for fundamental and first order modes versus core width with $t = 5.0\mu m$, $\lambda = 1.33\mu m$, $n_2(0) = 3.17$, $\Delta n_2(E) = 0.01$, $n_m = 0.394 + 8.2j$ and $n_1 = 3.5$.

change for the two SPP modes decreases as the core width increases, the rate of decrease for the first order mode being larger that the rate of decrease for

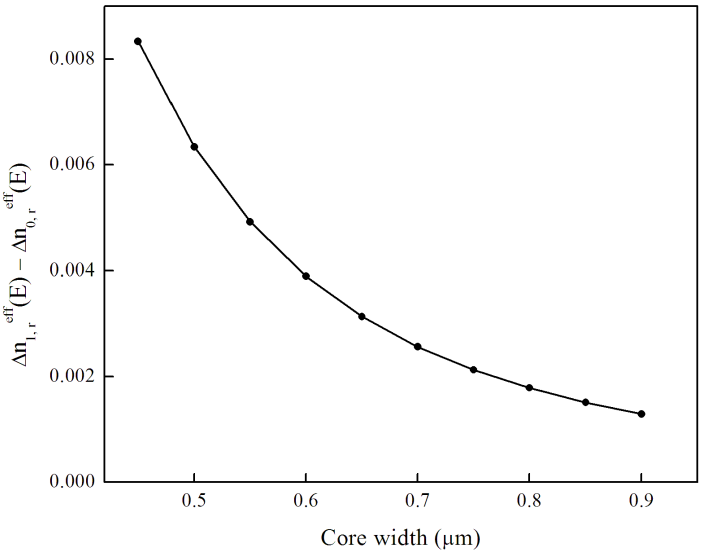

Figure 3.16: Difference of effective refractive index changes of fundamental and first order modes versus core width with $t = 5.0\mu m$, $\lambda = 1.33\mu m$, $n_2(0) = 3.17$, $\Delta n_2(E) = 0.01$, $n_m = 0.394 + 8.2j$ and $n_1 = 3.5$.

the fundamental mode. The difference of effective refractive index change for the SPP first order mode and fundamental mode ($\Delta n_{1,r}^{eff}(E) - \Delta n_{01,r}^{eff}(E)$) versus core width ($W_T$) is shown in Fig-3.16 for $t = 5.0\mu m$, $\lambda = 1.33\mu m$, $n_2(0) = 3.17$, $n_m = 0.394 + 8.2j$ and $n_1 = 3.5$. It is found that as W_T increases, ($\Delta n_{1,r}^{eff}(E) - \Delta n_{01,r}^{eff}(E)$) decreases. As the coupling length depends inversely on the difference of effective refractive index change of the two SPP modes ($L_C = \lambda/2[\Delta n_{1,r}^{eff}(E) - \Delta n_{0,r}^{eff}(E)]$), it is evident from the figure that the smaller is the core width W_T, the larger is the value of ($\Delta n_{1,r}^{eff}(E) - \Delta n_{01,r}^{eff}(E)$) and the smaller is the coupling length.

Fig-3.17 shows variation of the coupling length (L_C) of the device and the propagation length ($L_{P,m}$) of the two modes versus core width (W_T) with $t = 5.0\mu m$, $\lambda = 1.33\mu m$, $n_2(0) = 3.17$, $n_m = 0.394 + 8.2j$ and $n_1 = 3.5$. As W_T increases within the two-mode coupling region, the propagation lengths of fundamental and first order modes decreases almost linearly with a very slow rate, whereas the coupling length increases rapidly as the core width W_T increases in the two-mode coupling region. It is evident from the figure that, to achieve better performance of SPP device, the core width should be less than $\sim 0.496\mu m$ for which the coupling length is less than propagation length. So, we have chosen $W_T = 2w = 0.48\mu m$ for further study.

The variation of effective refractive index change ($\Delta n_{m,r}^{eff}(E)$) produced by applied optical pulse of energy E for fundamental and first order SPP modes

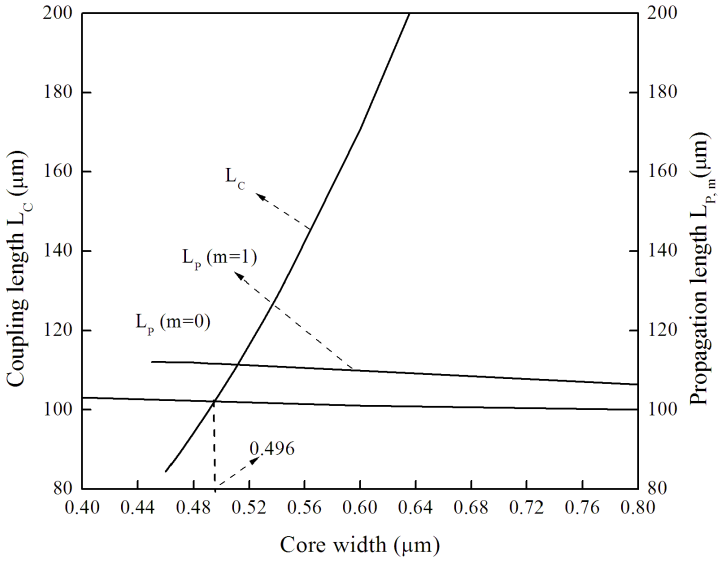

Figure 3.17: Coupling length and propagation length of the different modes versus core width within two mode coupling region with $t = 5.0\mu m$, $\lambda = 1.33\mu m$, $n_2(0) = 3.17$, $\Delta n_2(E) = 0.01$, $n_m = 0.394 + 8.2j$ and $n_1 = 3.5$.

with respect to changes in core thickness(t) are shown in Fig-3.18 for $W_T = 0.48\mu m$, $\lambda = 1.33\mu m$, $n_2(0) = 3.17$, $n_m = 0.394 + 8.2j$ and $n_1 = 3.5$. It is seen

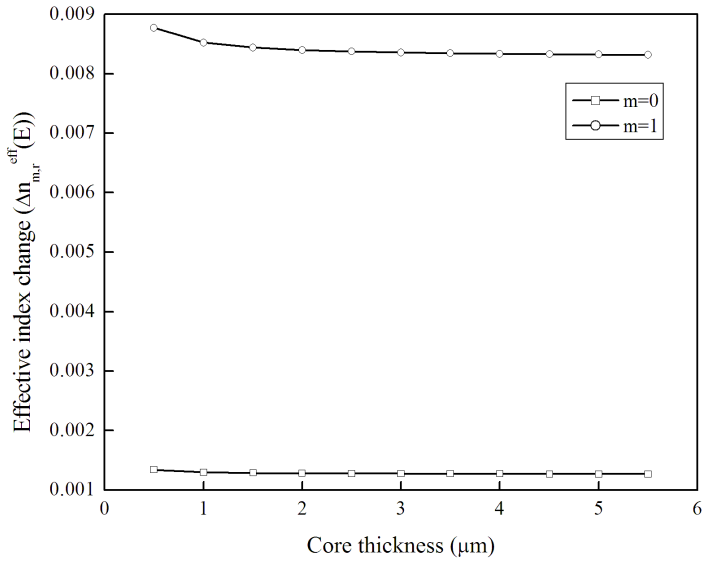

Figure 3.18: Effective refractive index change for fundamental and first order modes versus core thickness with $W_T = 0.48\mu m$, $\lambda = 1.33\mu m$, $n_2(0) = 3.17$, $\Delta n_2(E) = 0.01$, $n_m = 0.394 + 8.2j$ and $n_1 = 3.5$.

that effective refractive index change for the SPP fundamental mode is almost independent of any changes in the core thickness t, whereas effective refractive index change for the first order mode decreases very slowly with increase in t and can be approximated as constant for $t \geq 3\mu m$. It is also seen that the rate of

decrease of $\Delta n_{m,r}^{eff}(E)$ for the first order mode is larger that the rate of decrease of $\Delta n_{m,r}^{eff}(E)$ for the fundamental mode.

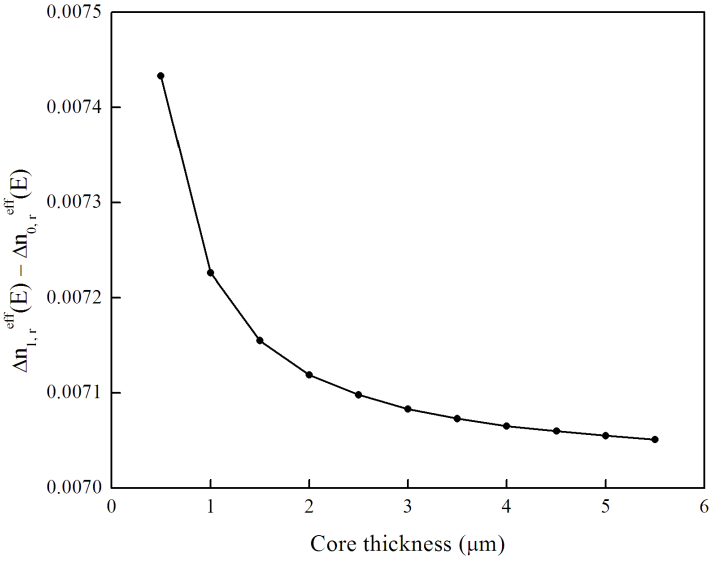

Figure 3.19: Difference of effective refractive index changes of fundamental and first order modes versus core thickness with $W_T = 0.48\mu m$, $\lambda = 1.33\mu m$, $n_2(0) = 3.17$, $\Delta n_2(E) = 0.01$, $n_m = 0.394 + 8.2j$ and $n_1 = 3.5$.

The difference of effective refractive index change for the SPP first oder mode and fundamental mode $(\Delta n_{1,r}^{eff}(E) - \Delta n_{01,r}^{eff}(E))$ versus core thickness (t) is shown in Fig-3.19 for $W_T = 0.48\mu m$, $\lambda = 1.33\mu m$, $n_2(0) = 3.17$, $n_m = 0.394$+$8.2j$ and $n_1 = 3.5$. It is found that as t increases, $(\Delta n_{1,r}^{eff}(E) - \Delta n_{01,r}^{eff}(E))$ decreases rapidly for smaller values of t and the decrease of $(\Delta n_{1,r}^{eff}(E) - \Delta n_{01,r}^{eff}(E))$ becomes almost linear for $t \geq 3\mu m$. It is evident from the figure that a very large value of core thickness t will contribute to increase in the device coupling length.

Fig-3.20 shows dependence of the coupling length (L_C) of the device and the propagation length $(L_{P,m})$ of the two modes on core thickness (t) for $W_T = 0.48\mu m$, $\lambda = 1.33\mu m$, $n_2(0) = 3.17$, $n_m = 0.394 + 8.2j$ and $n_1 = 3.5$. It is seen from the figure that, the propagation lengths of fundamental and first order modes increases with increase of core thickness t, whereas the coupling length remains almost constant as t increases. The propagation length becomes more than coupling length for $t > 4.61\mu m$. To achieve better performance of SPP device, the coupling length should be less than propagation length. So we have chosen $t = 5.0\mu m$ for further study. For $W_T = 0.48\mu m$ and $t = 5.0\mu m$, the beat length of the proposed device can be estimated as $\sim 2.98\mu m$.

The dependence of effective refractive index change for fundamental and first order modes $(\Delta n_{m,r}^{eff}(E),\ m = 0, 1)$ on change of refractive index of GaAsInP

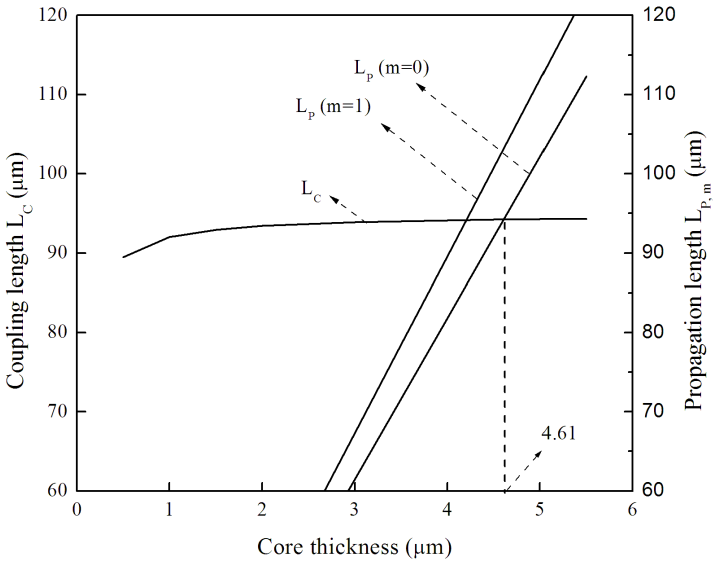

Figure 3.20: Coupling length and propagation length of the different modes versus core thickness within two mode coupling region with $W_T = 0.48\mu m$, $\lambda = 1.33\mu m$, $n_2(0) = 3.17$, $\Delta n_2(E) = 0.01$, $n_m = 0.394 + 8.2j$ and $n_1 = 3.5$.

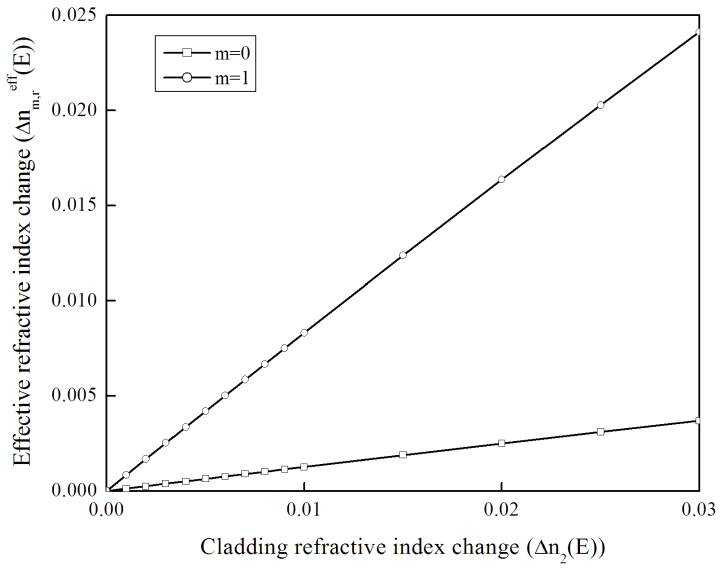

Figure 3.21: Effective refractive index change for fundamental and first order modes versus GaAsInP cladding refractive index change with $W_T = 0.48\mu m$, $t = 5.0\mu m$, $\lambda = 1.33\mu m$, $n_2(0) = 3.17$, $n_m = 0.394 + 8.2j$ and $n_1 = 3.5$.

cladding ($\Delta n_2(E)$) induced by optical pulse energy for $W_T = 0.48\mu m$, $t = 5.0\mu m$, $\lambda = 1.33\mu m$, $n_2(0) = 3.17$, $n_m = 0.394 + 8.2j$ and $n_1 = 3.5$ is shown in Fig-3.21. It is found that, as the change of refractive index of GaAsInP cladding due to applied optical pulse energy increases, the effective refractive index change for the two SPP modes increases, the rate of increases of the first order mode being more than that of the fundamental mode. Fig-3.22 shows the difference

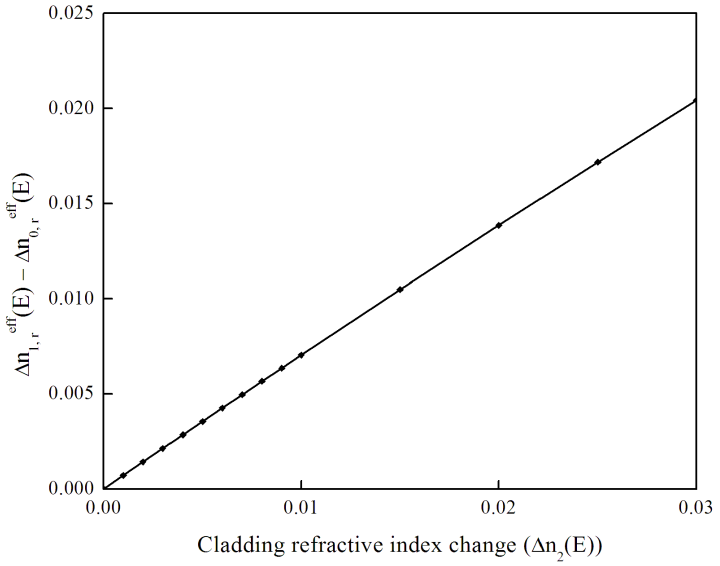

Figure 3.22: Difference of effective refractive index change of fundamental and first order modes versus GaAsInP cladding refractive index change with $W_T = 0.48\mu m$, $t = 5.0\mu m$, $\lambda = 1.33\mu m$, $n_2(0) = 3.17$, $n_m = 0.394 + 8.2j$ and $n_1 = 3.5$.

of effective refractive index change of first order mode and fundamental mode $(\Delta n_{1,r}^{eff}(E) - \Delta n_{0,r}^{eff}(E))$ versus refractive index change of GaAsInP cladding $(\Delta n_2(E))$ induced by applied optical pulse. It is seen that $(\Delta n_{1,r}^{eff}(E) - \Delta n_{0,r}^{eff}(E))$ increases as $\Delta n_2(E)$ increases. It is evident from the figure that larger is the change in refractive index of GaAsInP cladding, the smaller is the coupling length of the SPTMI device. Considering GaAsInP cladding refractive index change $\Delta n_2(E) = 0.01$, the coupling length for core width $W_T = 0.48\mu m$ and core thickness $t = 5.0\mu m$ is estimated from equation (3.17) as $L_C = 92.35\mu m$.

Fig-3.23 shows the dependence of phase change $\Delta\Phi(E)$ of the two propagating SPP modes induced by applied optical pulse on the energy of pulse applied for effective cross sectional area of GaAsInP cladding $A_{clad} = 1.0\mu m^2$, $1.5\mu m^2$, $2.0\mu m^2$, $2.5\mu m^2$ and $3.0\mu m^2$ obtained with $n_1 = 3.5$, $n_2(0) = 3.17$, $n_m = 0.394 + 8.2j$, $W_T = 0.48\mu m$, $t = 5.0\mu m$, $\lambda = 1.33\mu m$, $L_C = 92.35\mu m$ and $T_P = 1ps$. It is seen from the figure that as optical pulse energy E increases, $\Delta\Phi(E)$ increases. As the effective cladding area A_{clad} increases, $\Delta\Phi(E)$ decreases and the variation curve of $\Delta\Phi(E)$ in the figure also becomes closer and closer. For better optical pulse capturing in the cladding, we have chosen $A_{clad} = 2.0\mu m^2$ for which W_C is taken to be $0.2\mu m$. Moreover, for less area, the device size becomes compact. In the figure, optical pulse energy E required to get π phase change for $A_{clad} = 2.0\mu m^2$ is obtained as $E = 16.2pJ$.

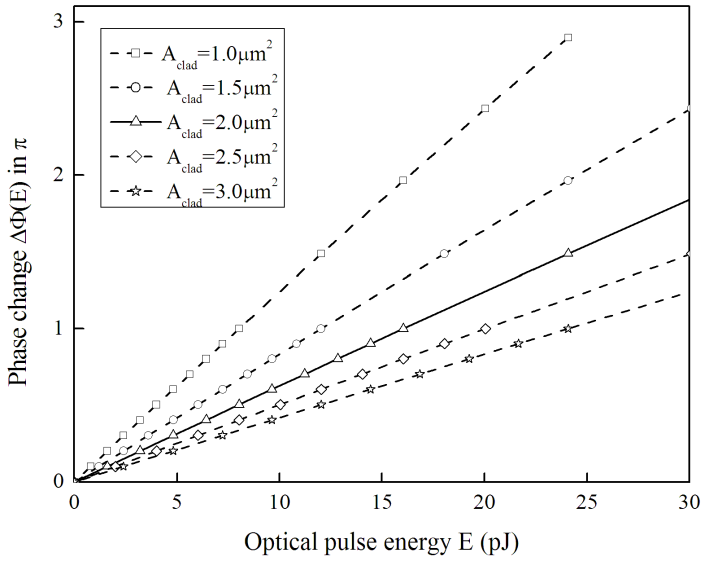

Figure 3.23: Phase change versus optical pulse energy for SPTMI coupler with $n_1 = 3.5$, $n_2(0) = 3.17$, $n_m = 0.394{+}8.2j$, $W_T = 0.48\mu m$, $t = 5.0\mu m$, $\lambda = 1.33\mu m$ and $L_C = 92.35\mu m$ and effective area of GaAsInP cladding $A_{clad} = 1.0\mu m^2$, $1.5\mu m^2$, $2.0\mu m^2$, $2.5\mu m^2$ and $3.0\mu m^2$

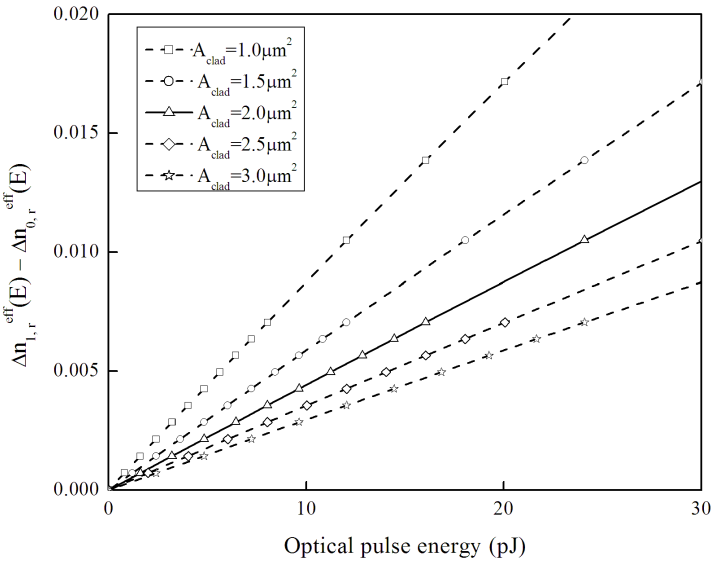

Figure 3.24: Difference of effective refractive index change for SPP fundamental and first order modes versus optical pulse energy for SPTMI coupler with $n_1 = 3.5$, $n_2(0) = 3.17$, $n_m = 0.394 + 8.2j$, $W_T = 0.48\mu m$, $t = 5.0\mu m$, $\lambda = 1.33\mu m$ and $L_C = 92.35\mu m$ and effective area of GaAsInP cladding $A_{clad} = 1.0\mu m^2$, $1.5\mu m^2$, $2.0\mu m^2$, $2.5\mu m^2$ and $3.0\mu m^2$

Fig-3.24 shows the difference of effective refractive index change $(\Delta n_{1,r}^{eff}(E) - \Delta n_{0,r}^{eff}(E))$ for SPP fundamental and first order modes versus optical pulse energy (E) for SPTMI coupler with $W_T = 0.48\mu m$, $t = 5.0\mu m$, $n_1 = 3.5$, $n_2(0) = 3.17$, $n_m = 0.394 + 8.2j$, $\lambda = 1.33\mu m$ and $L_C = 92.35\mu m$ and different

area of GaAsInP cladding $A_{clad} = 1.0\mu m^2$, $1.5\mu m^2$, $2.0\mu m^2$, $2.5\mu m^2$ and $3.0\mu m^2$. It is found that $(\Delta n_{1,r}^{eff}(E) - \Delta n_{0,r}^{eff}(E))$ increases with increase in optical pulse energy E. So, larger is the energy of applied optical pulse, the higher is phase change.

3.4.3 Power transferred to output waveguides

Considering input field launched through only on input access waveguide, the power transferred to output access waveguides at a distance $z = L$ with application of optical pulse of energy E can be written as follows:
Power transferred to output access waveguide-3 i.e., the normalized bar state power is given as

$$\frac{P_3}{P_1} = \left| \frac{H_3(x, L, E)}{H_1(x, 0)} \right|^2 \tag{3.19}$$

and power transferred to output access waveguide-4, or the normalized cross state power is given as

$$\frac{P_4}{P_1} = \left| \frac{H_4(x + w, L, E)}{H_1(x, 0)} \right|^2 \tag{3.20}$$

where, $H_1(x, 0)$ is the input field incident at the input access waveguide-1 at $z = 0$ and $H_3(x, L, E)$ and $H_4(x + w, L, E)$ are the output field at output access waveguides 3 and 4 respectively at a coupling distance $z = L$. Equations (3.19) and (3.20) for the surface plasmonic TMI coupler can also be written as

$$\frac{P_3}{P_1} = \cos^2\left(\frac{\Delta\Phi_T(E)}{2}\right) \exp[-2(\beta_0^{im}(n_2(E)) - \beta_1^{im}(n_2(E))L] \tag{3.21}$$

$$\frac{P_4}{P_1} = \sin^2\left(\frac{\Delta\Phi_T(E)}{2}\right) \exp[-2(\beta_0^{im}(n_2(E)) - \beta_1^{im}(n_2(E))L] \tag{3.22}$$

where, $\Delta\Phi_T(E) = (\beta_0^r(E) - \beta_1^r(E))L$ is the phase difference between the two SPP fundamental and first order modes at a distance $z = L$.

The dependence of the normalized cross state power (P_4/P_1) and normalized bar state power (P_3/P_1) on the coupling distance L is shown in Fig-3.25 with $W_T = 0.48\mu m$, $t = 5.0\mu m$, $n_1 = 3.5$, $n_2(0) = 3.17$, $n_m = 0.394 + 8.2j$ and $\lambda = 1.33\mu m$. It is found that, as the coupling distance L increases, P_4/P_1 and P_3/P_1 shows a periodic variation. It is evident from the figure that the device shows cross state coupling for coupling distance $L = 86.4\mu m$, $92.35\mu m$,

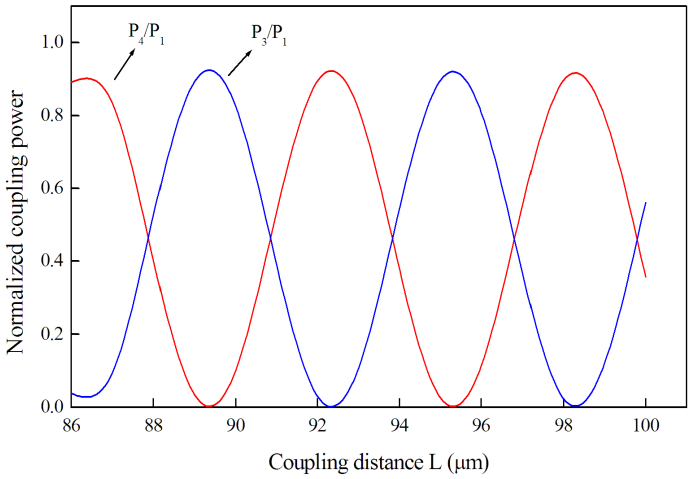

Figure 3.25: Normalized cross state power (P_4/P_1) and bar state power (P_3/P_1) vs coupling distance L for SPTMI coupler with $W_T = 0.48\mu m$, $t = 5.0\mu m$, $n_1 = 3.5$, $n_2(0) = 3.17$, $n_m = 0.394 + 8.2j$ and $\lambda = 1.33\mu m$.

$98.3\mu m$ etc. where, all the power is transferred to waveguide-4 and no power is coupled to waveguide-3. On the other hand, the device shows bar state coupling for $L = 89.38\mu m$, $95.35\mu m$ etc. where, all the coupled power is transferred to waveguide-3 and no power is coupled to waveguide-4. The normalized peak output power of both P_4/P_1 and P_3/P_1 decays exponentially with increase in the coupling distance L. We have chosen $L = 92.35\mu m$ as the length of coupling region for the SPTMI coupler with core width $W_T = 0.48\mu m$ and core thickness $t = 5.0\mu m$ which corresponds to cross state coupling of the device and is very close to the coupling length of the device estimated for GaAsInP cladding refractive index change $\Delta n_2(E) = 0.01$. It is about ~ 8.4 times less than that of optically-controlled TMI coupler [122], ~ 13.7 times less than that of nonlinear directional coupler based MMI coupler [120] and ~ 22.4 times less than that of MZ based MMI-TMI all optical device [118] reported by previous researchers.

Fig-3.26 shows variation of the normalized cross state power (P_4/P_1) and normalized bar state power (P_3/P_1) for the SPTMI device versus applied optical pulse energy E with $W_T = 0.48\mu m$, $t = 5.0\mu m$, $L = 92.35\mu m$ (cross state coupling), $n_1 = 3.5$, $n_2(0) = 3.17$, $n_m = 0.394+8.2j$ and $\lambda = 1.33\mu m$ for effective cladding area $A_{clad} = 2.0\mu m^2$, $2.5\mu m^2$ and $3.0\mu m^2$. It is seen from the figure that at $E = 0pJ$, the power is fully transferred to waveguide-4 (cross state) and no power is coupled to waveguide-3. The power remains at waveguide-3 (bar state) by launching of optical pulse of energy $E = 16.4pJ$ for $A_{clad} = 2.0\mu m^2$. For $A_{clad} = 2.5\mu m^2$ and $3.0\mu m^2$, optical pulse energy required to get full transfer of power to waveguide-3 are $E = 20.5pJ$ and $24.6pJ$ respectively. This transfer

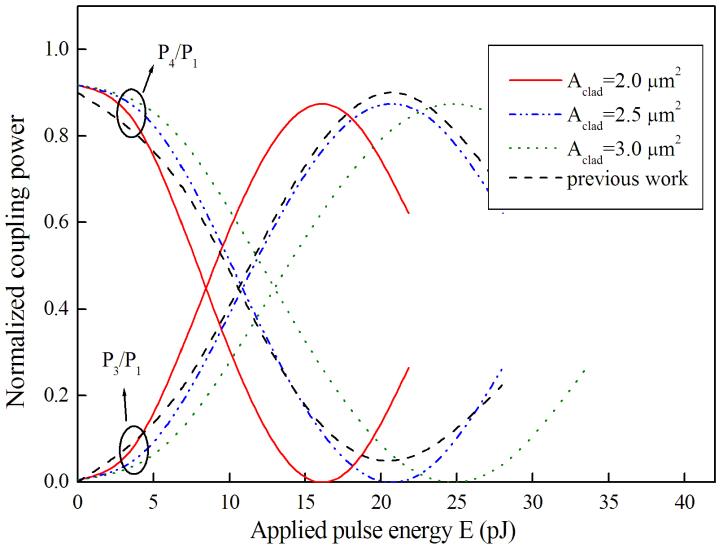

Figure 3.26: Normalized cross state power (P_4/P_1) and bar state power (P_3/P_1) versus optical pulse energy E for the SPTMI coupler with $W_T = 0.48\mu m$, $t = 5.0\mu m$, $L = 92.35\mu m$ (cross state), $n_1 = 3.5$, $n_2(0) = 3.17$, $n_m = 0.394 + 8.2j$ and $\lambda = 1.33\mu m$ and different cladding area $A_{clad} = 2.0\mu m^2$, $2.5\mu m^2$ and $3.0\mu m^2$ and a previously reported device with $L = 778.5\mu m$ and $A_{clad} = 0.8\mu m^2$.

of power from waveguide-4 to waveguide-3 is due to change in refractive index of cladding region (made of GaAsInP) and no significant change in refractive index in core region (made of silicon) with application of optical pulse. As area A_{clad} increases, optical pulse energy required to get full transfer of power from waveguide-4 to waveguide-3 increases. So we have chosen $A_{clad} = 2.0\mu m^2$ for further study. Fig-3.26 also shows variation of the normalized coupling power for an optically-controlled TMI (OTMI) device [122] reported previously without using surface plasmonic waveguide. It is seen that optical pulse energy E required to get full transfer of power to waveguide-3 for $A_{clad} = 2.0\mu m^2$ is ~ 1.3 times less than that of OTMI device [122] reported previously without using SPP structure. This is because the effect of cladding index change on SPP mode propagation is more than that on excited modes propagated in OTMI coupler. Although small amount of optical pulse energy is penetrated into core region due to reflection at core-GaAsInP cladding interface, this do not change much refractive index of silicon core because of the small nonlinear refractive index change of silicon core in comparison to GaAsInP cladding. Optical pulses of width $T_P \sim 1ps$ and energy $E = 16.4pJ$ required for refractive index modulation in GaAsInP cladding can be generated by KCl:Tl^0(1) color-center laser (discussed in section 2.4.5 of chapter 2) using coupled cavity mode locking [124].

We have also studied the dependence of normalized cross state power

(P_4/P_1) and normalized bar state power (P_3/P_1) of the SPTMI device on applied optical pulse energy E for bar state coupling and 3dB coupling. Fig-3.27 shows variation of the normalized coupling power of the SPTMI device versus applied optical pulse energy E with $W_T = 0.48\mu m$, $t = 5.0\mu m$, $n_1 = 3.5$, $n_2(0) = 3.17$, $n_m = 0.394 + 8.2j$, $\lambda = 1.33\mu m$ and $L = 95.35\mu m$ for bar state coupling for different cladding area $A_{clad} = 2.0\mu m^2$, $2.5\mu m^2$ and $3.0\mu m^2$. It is seen from the

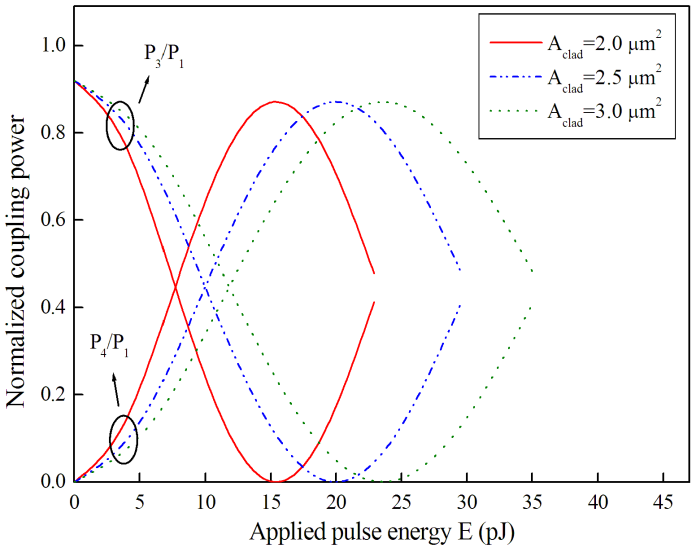

Figure 3.27: Normalized cross state power (P_4/P_1) and bar state power (P_3/P_1) versus optical pulse energy E for the SPTMI coupler with $W_T = 0.48\mu m$, $t = 5.0\mu m$, $L = 95.35\mu m$ (bar state), $n_1 = 3.5$, $n_2(0) = 3.17$, $n_m = 0.394 + 8.2j$ and $\lambda = 1.33\mu m$ and different cladding area $A_{clad} = 2.0\mu m^2$, $2.5\mu m^2$ and $3.0\mu m^2$.

figure that at $E = 0pJ$, the power is fully transferred to waveguide-3 (bar state) and the power is fully transferred to waveguide-4 (cross state) on launching of optical pulse of energy $E = 15.9pJ$, $19.8pJ$ and $23.8pJ$ for $A_{clad} = 2.0\mu m^2$, $2.5\mu m^2$ and $3.0\mu m^2$ respectively. The optical pulse energy required to change bar state coupling to cross state coupling increases as area A_{clad} increases. From Fig-3.26 and Fig-3.27, it is also seen that the optical pulse energy required to change cross state coupling to bar state coupling and vice versa is larger for device with smaller length.

It is seen from Fig-3.25 that the output power is distributed equally in the output waveguides for coupling length $L = 93.85\mu m$. Fig-3.28 shows variation of the normalized coupling power of the SPTMI device versus applied optical pulse energy E with $W_T = 0.48\mu m$, $t = 5.0\mu m$, $n_1 = 3.5$, $n_2(0) = 3.17$, $n_m = 0.394+8.2j$ and $\lambda = 1.33\mu m$ for device length $L = 93.85\mu m$ corresponding to 3dB coupling with different cladding area $A_{clad} = 2.0\mu m^2$, $2.5\mu m^2$ and $3.0\mu m^2$. For

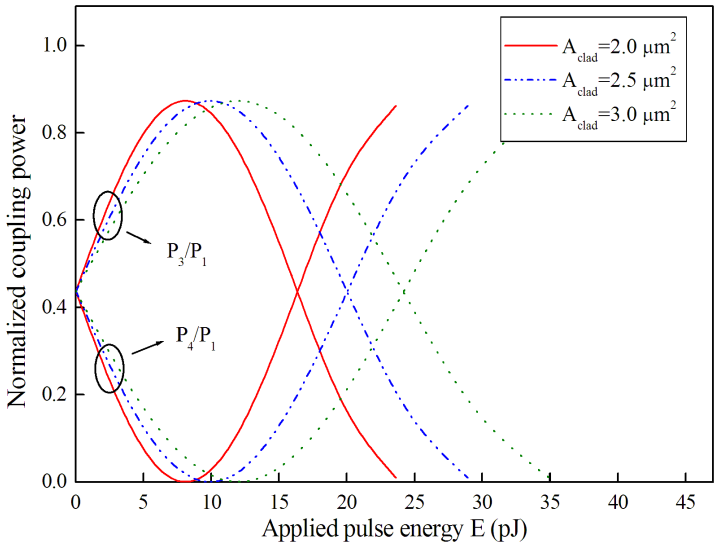

Figure 3.28: Normalized cross state power (P_4/P_1) and bar state power (P_3/P_1) versus optical pulse energy E for the SPTMI coupler with $W_T = 0.48\mu m$, $t = 5.0\mu m$, $L = 93.85\mu m$ (3dB coupling), $n_1 = 3.5$, $n_2(0) = 3.17$, $n_m = 0.394 + 8.2j$ and $\lambda = 1.33\mu m$ and different cladding area $A_{clad} = 2.0\mu m^2$, $2.5\mu m^2$ and $3.0\mu m^2$.

$E = 0$, the device shows 3dB coupling i.e., the output power is distributed equally between the output waveguides. As the energy of optical pulse is increased, the output power is gradually coupled to the output waveguide-3 and the device is in bar state. The device comes to the 3dB state on further increase of optical pulse energy for $E = 16.1pJ$, $20.2pJ$ and $24.2pJ$ for $A_{clad} = 2.0\mu m^2$, $2.5\mu m^2$ and $3.0\mu m^2$ respectively.

3.4.4 Total length of SPTMI coupler

The total length of the device is the combined length of the coupling region and the transition length of the input and output access waveguides as shown in Fig-3.29. From Fig-3.29, the relation between the transition length (L_T), bending

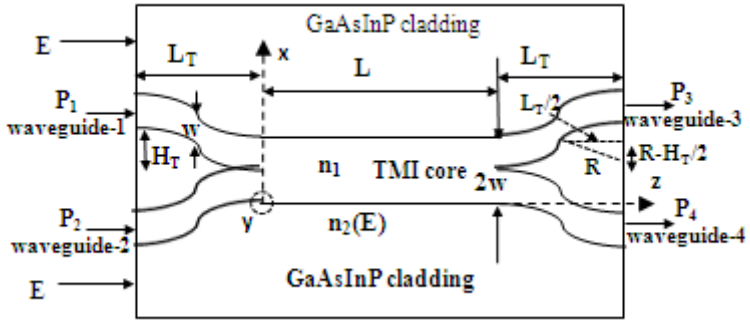

Figure 3.29: Top schematic view of SPTMI coupler

height (H_T) and bending radius (R) can be expressed as

$$\begin{aligned} R^2 &= \left(\frac{L_T}{2}\right)^2 + \left(R - \frac{H_T}{2}\right)^2 \\ \text{or,} \quad \left(\frac{L_T}{2}\right)^2 &= R^2 - \left(R - \frac{H_T}{2}\right)^2 \\ \text{or,} \quad \frac{L_T^2}{4} &= RH_T - \frac{H_T^2}{4} \\ \text{or,} \quad L_T^2 &= H_T\left(4R - H_T\right) \\ \text{or,} \quad L_T &= \sqrt{H_T\left(4R - H_T\right)} \end{aligned} \tag{3.23}$$

The bending height H_T is very small compared to the bending radius R ($H_T << R$). Thus the expression (3.23) for the transition length L_T can be written as

$$L_T \approx \sqrt{4H_T R} \tag{3.24}$$

On the other hand, the S-bending loss for input and access waveguides corresponding to bending height H_T and bending radius R can be estimated with the following expression [122]

$$\text{S-bending loss} = 8.686\alpha R \cos^{-1}\left[1 - \frac{H_T}{2R}\right] \tag{3.25}$$

where α is the loss coefficient depending on R and can be estimated as $\alpha = 3.997 \times 10^{-6}$ [122].

In case of a waveguide bend, the smaller is the bending radius, the sharper is the bend, and the sharper is the bend, the larger is the bending loss. Thus,

a smaller bending radius R provides a large bending loss. But, from equation (3.24), it is seen that a larger value of bending radius R gives a larger transition length L_T and thus contributes to an increase in the device length. Considering a bending radius of $R = 39\mu m$ and access waveguide S-bending loss of $\sim 0.1dB$, the bending height can be estimated from equation (3.25) as $H_T = 4\mu m$.

Thus, we have taken $R = 39\mu m$ and $H_T = 4\mu m$ for S-bending loss of 0.1dB. The transition length of the input and output access waveguides can be estimated as

$$L_T \approx \sqrt{4 \times 4 \times 39} \approx 24.97\mu m$$

and the total device length can be estimated as

$$L_D = L + 2L_T \approx 92.35 + 2 \times 24.97 \approx 142.29\mu m$$

where, $L = 92.35\mu m$ is the coupling length as mentioned in section 3.4. The total length of the device is found to be about ~ 5.9 times compact than the OTMI coupler [122] based device reported previously without using SPP structure.

The S-bending loss for input and access waveguides corresponding to bending height H_T and bending radius R is given by equation (3.25). Considering bending radius of $R = 39\mu m$ and bending height of $H_T = 4\mu m$, the S-bending loss can be estimated as

$$\begin{aligned} \text{S-bending loss} &= 8.686 \times \left(3.997 \times 10^{-6}\right) \times 39 \times \cos^{-1}\left[1 - \frac{4}{2 \times 39}\right] \\ &\approx 0.1dB \end{aligned}$$

3.4.5 Fabrication tolerance

Since the precise fabrication of a device structure with exact design parameters may be difficult, it is required to study the performance degradation of the device with small unwanted variations in the device parameters. We have studied the effect of fabrication tolerances of core width (δw) of the proposed device on power imbalance ($= 10\log_{10} P_3/P_4$). The variation of the power imbalance ($10\log_{10} P_3/P_4$) with respect to deviations in core width (δw) with $W_T = 0.48\mu m$, $t = 5.0\mu m$, $L = 92.35\mu m$ (cross state coupling), $n_1 = 3.5$, $n_2(0) = 3.17$, $n_m = 0.394 + 8.2j$ and $\lambda = 1.33\mu m$ for the SPTMI coupler is shown in Fig-3.30. From the figure, the minimum power imbalance is obtained as $\sim -47.3dB$ at $\delta w = 0$.

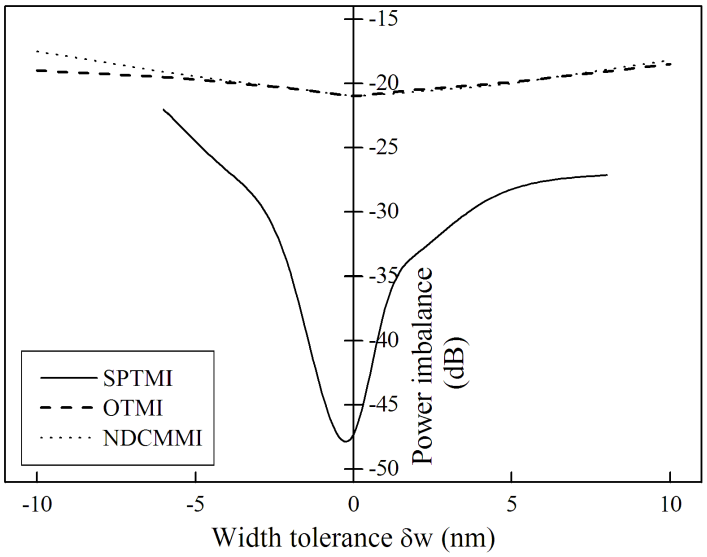

Figure 3.30: Power imbalance ($10\log_{10} P_3/P_4$) versus width tolerance (δw) for SPTMI coupler with $W_T = 0.48\mu m$, $t = 5.0\mu m$, $L = 92.35\mu m$ (cross state coupling), $n_1 = 3.5$, $n_2(0) = 3.17$, $n_m = 0.394 + 8.2j$ and $\lambda = 1.33\mu m$ and for existing works.

For small variations in the core width, the power imbalance increases almost symmetrically on both sides of the minimum for any positive or negative changes in the width tolerance δw.

Fig-3.30 also shows the power imbalance characteristics for previously reported works based on OTMI coupler [122] and nonlinear directional coupler based MMI (NDCMMI) coupler [120]. Although the power imbalance variation due to deviation of waveguide width (δw) in optically-controlled TMI (OTMI) coupler and NDCMMI coupler are less than that of proposed SPTMI coupler, the minimum power imbalance of the SPTMI coupler is ~ 2.24 times less than that of previous works [120, 122].

3.4.6 Optical power launching efficiency

The optical power launching efficiency is defined as the amount of optical power emitted from the source that can be coupled into a fiber and can be expressed as the ratio of the power coupled into the fiber to the power emitted from the source [126]. For launching of input power in the access waveguide core and optical pulse into the cladding region, optical fibers of core radius r are used, as shown in Fig-3.31.

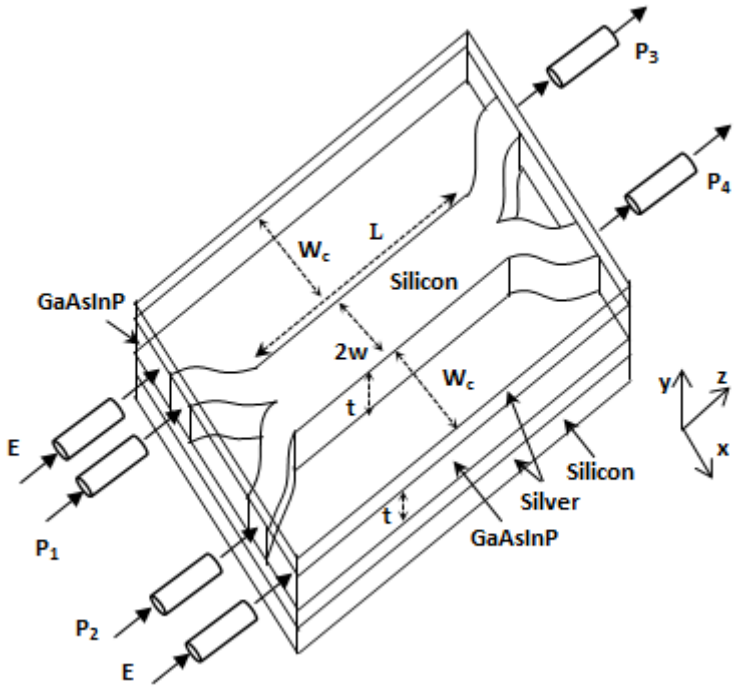

Figure 3.31: 3D schematic view of SPTMI coupler showing power launching by optical fiber.

Optical power launching efficiency to waveguide core

The optical power launching efficiency to waveguide core via optical fiber of core radius r can be written as [126]

$$\eta_{core} = \frac{A_{core}}{\pi r^2}(NA_{core})^2 \tag{3.26}$$

where, A_{core} is the cross sectional area of access waveguide core and NA_{core} is the numerical aperture of core written as

$$NA_{core} = \sqrt{n_1^2 - n_{m,real}^2} \tag{3.27}$$

Here, $n_1 = 3.5$ and $n_{m,real} = 0.394$. The cross sectional area of access waveguide core can be estimated as $A_{core} = (0.24 \times 5.0)\mu m^2 = 1.2\mu m^2$. Hence the optical power launching efficiency to waveguide core via optical fiber of core radius $r = 2.2\mu m$ can be estimated as

$$\begin{aligned} \eta_{core} &= \frac{1.2}{3.14 \times 2.2^2} \times (3.5^2 - 0.394^2) \\ &= \frac{1.2}{3.14 \times 4.84} \times 12.09476 \\ &\approx 0.955 \end{aligned}$$

Optical power launching efficiency to GaAsInP cladding

The optical power launching efficiency to GaAsInP cladding via optical fiber of core radius r can be written as [126]

$$\eta_{clad} = \frac{A_{clad}}{2\pi r^2}(NA_{clad})^2 \tag{3.28}$$

where, A_{clad} is the effective cross sectional area of GaAsInP cladding and NA_{clad} is the numerical aperture of GaAsInP cladding written as

$$NA_{clad} = \sqrt{n_2(0)^2 - n_{m,real}^2} \tag{3.29}$$

Here, $n_2(0) = 3.17$, $n_{m,real} = 0.394$ and the effective cross sectional area of GaAsInP cladding, $A_{clad} = 2.0\mu m^2$. Hence the optical power launching efficiency to GaAsInP cladding via optical fiber of core radius $r = 1.8\mu m$ can be estimated as

$$\begin{aligned} \eta_{clad} &= \frac{2.0}{2 \times 3.14 \times 1.8^2} \times (3.17^2 - 0.394^2) \\ &= \frac{2.0}{2 \times 3.14 \times 3.24} \times 9.89366 \\ &\approx 0.972 \end{aligned}$$

3.5 Values of device parameters of the proposed device

We have introduced a compact surface plasmonic two-mode interference (SPTMI) coupler as a basic component for integrated optical processor devices. The design parameters of the proposed SPTMI device are summarized in the Table-3.2 given below.

The proposed structure has been able to address the disadvantages in the previously reported integrated optic devices such as large device size [118–122], high power consumption [119, 122] and instability [127, 128]. The advantages of the proposed SPTMI coupler over few previously reported devices are discussed below:

1. **Compact device size:** The proposed structure has a compact device dimension which is necessary for the large scale integration of integrated optic devices for present day's high speed communication system. The

Table 3.2: Device parameters for the proposed device

Device parameters	Values
Core (Silicon) refractive index (n_1)	3.5
Metal cladding (Silver) refractive index (n_m)	$0.394 + 8.2j$
Side cladding (GaAsInP) refractive index ($n_2(0)$)	3.17
Nonlinear coefficient of GaAsInP (n_{nl})	$-2 \times 10^{-3} \mu m^2 W^{-1}$
Core width ($2w$)	$0.48 \mu m$
Core thickness (t)	$5.0 \mu m$
GaAsInP cladding width (W_C)	$0.2 \mu m$
Effective cladding (GaAsInP) area (A_{clad})	$2.0 \mu m^2$
Energy of applied optical pulse (E)	$16.4 pJ$
Full width at half maximum of optical pulse (T_P)	$1 ps$
Bending radius of access waveguides (R)	$39 \mu m$
Bending height of access waveguides (H_T)	$4 \mu m$
Transition length of access waveguides (L_T)	$24.97 \mu m$
Length of coupling region (L)	$92.35 \mu m$
Total device length	$142.29 \mu m$

length of the coupling region is $L = 92.35 \mu m$ which is about ~ 8.4 times less than that of optically-controlled TMI coupler [122], ~ 13.7 times less than that of nonlinear directional coupler based MMI coupler [120] and ~ 22.4 times less than that of MZI and MMI-TMI based all optical device [118]. The total length of the device is obtained as $L_D = 142.29 \mu m$ which is ~ 5.9 times compact than that of OTMI coupler [122].

2. **High operating speed:** As the recovery time of refractive index change of GaAsInP cladding with application of optical pulse is $\sim 1ps$, a switching time of the order of picoseconds is expected.

3. **Low power consumption:** The power consumption in the SPTMI coupler is $\sim 16.4pJ$ which is close to optical pulse energy required for switching of coupling states. This is about ~ 1.3 times less than the power consumption in a similar work reported previously without using SPP structure [122].

4. **Stability:** The disadvantages such as difficulty in precise control of input phase difference [127] or unwanted thermo-optic effects [128] leading to instability does not occur in the proposed structure.

5. **High fabrication tolerance:** The power imbalance of the proposed device is found to be very small ($\sim -47.3dB$). Although the power imbalance variation of the proposed device due to deviation of waveguide width (δw) is higher than those in NDCMMI coupler [120] and optically-controlled TMI (OTMI) coupler [122], the minimum power imbalance of the SPTMI coupler is ~ 2.24 times less than that of previous works. Moreover, the power imbalance of the proposed coupler for δw variation in the range $|\delta w| \leq 8\mu m$ is seen to be less than the power imbalance corresponding to $\delta w = 0$ for the previously reported devices [120, 122] .

3.6 Conclusion

In this chapter, a 2×2 compact two-mode interference coupler based on surface plasmoic waveguide has been proposed as a basic component of integrated optical processor devices. The mode propagation in SPP based TMI waveguide is analyzed with the help of mathematical model based on effective index methods. The proposed structure consists of silicon core, silver upper and lower cladding and GaAsInP left and right cladding. The refractive index of GaAsInP shows a nonlinear refractive index change on application of optical pulse energy. By modulating the refractive index of GaAsInP cladding with incidence of optical pulse, an additional phase change can be introduced between the excited SPP modes propagating through the silicon core.

The optical pulse dependent coupling characteristics of the SPTMI coupler is studied with the help of the mathematical model. The optical pulse energy required to change cross state coupling to bar state coupling is found to be $16.4pJ$ which is ~ 1.3 times lower than that in a previously reported work [122]. The coupling length of the proposed device is estimated as $92.35\mu m$ which is about ~ 8.4 times [122], ~ 13.7 times [120] and ~ 22.4 times [118] less than previously reported works, whereas the total length of the device ($L_D = 142.29\mu m$) is ~ 5.9 times compact than that of previous work [122]. The device is found to show a very low cross talk ($\sim -47.3dB$) which is ~ 2.24 times less than previously reported devices [120, 122]. With the help of this basic SPTMI coupler, operation of all-optical fundamental logic gates and optically tunable power splitter

are shown in chapter 4 and chapter 5 respectively.